Influence of Aluminum Incorporation on Iron Oxide Nanoparticles for High Frequency Applications

Saira Riaz[1)], Asif Hussain[2)], Yan-Jun Guo[3)], *M Khaleeq-ur-Rehman[4)] and Shahzad Naseem[5]

[1), 2), 4), 5)] *Centre of Excellence in Solid State Physics, University of Punjab, Lahore, Pakistan*
[3)] *National Center for Nanoscience & Technology, CAS, Beijing, 100190, China*
[1)] saira_cssp@yahoo.com

ABSTRACT

Among various metal oxides, iron oxide is the material of interest due to its high stability, narrow band gap (2.2eV) and its semiconducting properties (Riaz et al. 2013, Rivera et al. 2013). We here report synthesis of aluminum doped iron oxide nanoparticles using sol-gel method. Dopant concentration is varied as 2%-10%. XRD results confirm the formation of hematite phase of iron oxide. Shift in XRD peak position to slightly higher angles indicate successful incorporation of aluminum in the host lattice. Al^{3+} has six-coordinate ionic radius of 67.5pm that is smaller than Fe^{3+} ions (74pm). So, decrease in lattice spacing and unit cell volume is observed with increase in dopant concentration. Dielectric constant slightly decreases as frequency of applied field increases in low frequency region. Sharp increase in dielectric constant in high frequency region (>10MHz) is attributed to space charge polarization. Presence of aluminum cations gives rise to their displacement in externally applied electric field that also contributes to polarization and hence dielectric constant. Tangent loss on the other hand decreases as frequency of applied field increases and becomes constant in high frequency region. Decrease in loss and increase in dielectric constant of Al doped iron oxide nanoparticles makes them a potential candidate for high frequency applications.

1. INTRODUCTION

Nanomaterials with tailorable magnetic, dielectric and magneto-dielectric properties are promising candidates for frequency-based applications including microwave communication, radar and antenna systems. The desired features for these applications include: 1) Small size, 2) Wide operating bandwidth; 3) High efficiency. In case of antenna applications wave impedance and miniaturization factor both depend on the relative dielectric constant and relative permeability. This means a wider bandwidth along with scaling down of the material and high dielectric constant are extremely crucial for such high frequency applications. In addition, the material used for these applications must have a very low loss factor (Yang et al. 2010).

Among various materials of interest hematite is a promising candidate owing to its chemical and temperature stability. Hematite (α-Fe_2O_3) is one of the most common oxides in earth. It crystallizes in rhombohedral lattice with R3c space group under ambient conditions. It can be described in two ways: 1) Rhombohedral structure with

a=b=c=5.43Å and angel between the two edges given as 55.18˚. It consists of two formula units: 2) Hexagonal structure with a =5.03Å and c = 13.75Å (Riaz et al. 2014, Akbar et al. 2014). The lattice is composed of hexagonal closed packed octahedral array of oxygen anions in which every fourth available octahedral site is occupied by iron cations (Chakraborty et al. 2016, Aragon et al. 2016).

Hematite exhibits antiferromagnetic Neel temperature of 955K. Below Neel temperature it exhibits antiferromagnetic insulating behavior. However, above Morin temperature (260K), hematite shows weak ferromagnetic behavior. As temperature is reduced below 260K perfectly antiparallel arrangements of spins occur in the same plane while perfectly antiparallel arrangement of spins arises with the adjacent planes. Above Morin temperature hematite arranges itself in the form of layers of Fe^{3+} cations. Because of spin-orbit coupling canting of the spins between the adjacent planes arises that results in weak ferromagnetic behavior in otherwise antiferromagnetic hematite (Akbar et al. 2014, Glasscock et al. 2008).

Despite chemical and thermal stability of hematite, very little attention is devoted to study hematite especially the investigation of dielectric properties is extremely limited. We here report preparation of aluminum doped hematite nanoparticles prepared using sol-gel method. Dopant concentration was varied as 4%, 6% and 8%. Changes in structural and dielectric properties are correlated with changes in dopant concentration.

2. EXPERIMENTAL DETAILS

Aluminum doped iron oxide nanoparticles were prepared using low cost and application oriented sol-gel method. For this purpose, iron nitrate was used as precursor and water and ethylene glycol as solvents. Iron nitrate was dissolved in water and ethylene glycol and heated on hot plate to obtain iron oxide sol. Details of sol-gel synthesis were reported earlier (Riaz et al. 2014, Akbar et al. 2014). For aluminum doping, aluminum nitrate was dissolved in ethylene glycol and was added to iron oxide sol. Dopant concentration was varied as 4%, 6% and 8%. These sols were then heat-treated to obtain aluminum doped iron oxide nanoparticles.

These nanoparticles were structurally characterized using Bruker D8 Advance X-ray diffractometer. Dielectric properties were studied with the help of 6500B Precision Impedance Analyzer under parallel plate configuration.

3. RESULTS AND DISCUSSION

Fig. 1 shows XRD patterns of aluminum doped iron oxide nanoparticles prepared using sol-gel method. Presence of diffraction peaks corresponding to planes (104), (110), (113), (024), (106), (214) and (300) indicated the formation of phase pure hematite. No peaks corresponding to aluminum oxide were observed even at high dopant concentration of 8% indicating that dopant atoms have been successfully incorporated in the host lattice. Ratio of ionic radius of Al^{3+} and Fe^{3+} is 0.912 (~1). This value is much high as compared to 0.59 that is the criteria for synthesis of interstitial solid solution (Riaz *et al.* 2014, Riaz et al. 2015, Kumari et al. 2015). Therefore, the probability that aluminum ions occupy interstitial sites is extremely low. Shift in XRD peaks' positions to slightly higher angles indicates successful incorporation of aluminum in the host lattice. However, it can be seen that as dopant concentration was

increased beyond 6% crystallinity of nanoparticles decreases indicated by decrease in peak intensities. At high dopant concentration the probability that dopant atoms sit on the grain boundaries increases. This results in destruction of crystalline order as can be seen in Fig. 1 at dopant concentration of 8%.

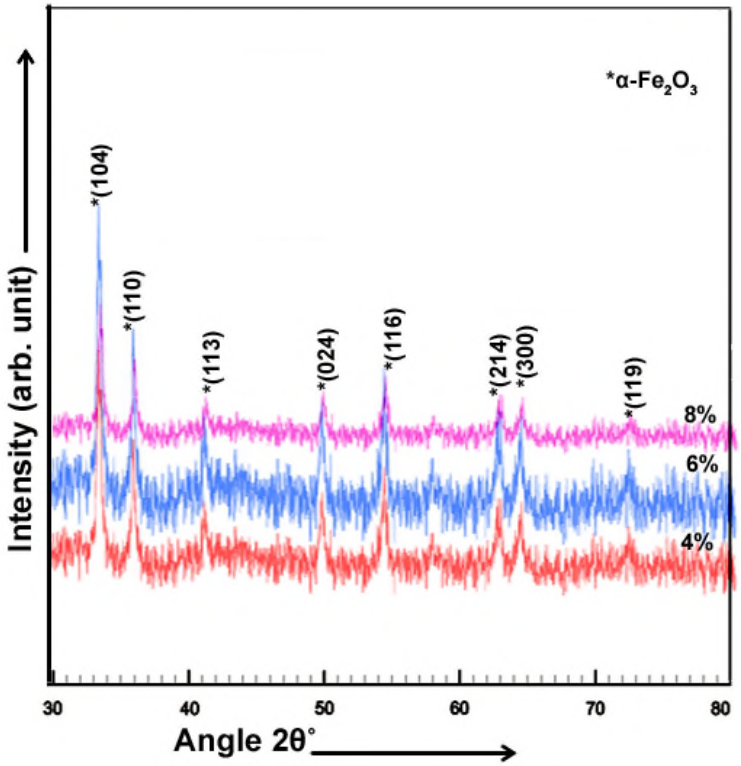

Fig. 1 XRD patterns for aluminum doped iron oxide nanoparticles

Crystallite size (*t*) (Cullity 1956), dislocation density (*δ*) (Kumar et al. 2011) and lattice parameters (Cullity 1956) were calculated using Eqs. 1-3.

$$t = \frac{0.9\lambda}{B\cos\theta} \tag{1}$$

$$\delta = \frac{1}{t^2} \tag{2}$$

$$\sin^2\theta = \frac{\lambda^2}{3a^2}\left(h^2 + k^2 + hk\right) + \frac{\lambda^2 l^2}{4c^2} \tag{3}$$

Where, *θ* is the diffraction angle, λ is the wavelength (1.5406Å) and *B* is Full Width at Half Maximum. δ stands for dislocation density. Crystallite size and dislocation density are plotted as a function of dopant concentration in Fig. 2. Crystallite size increased from 22.5nm to 23.56nm as dopant concentration was increased from 4% to 6%. Further increase in dopant concentration resulted in decrease in crystallite size and increase in dislocation density. Increase in crystallite size at low dopant concentration

suggests that dopant atoms are fully dissolved in the host lattice (Riaz et al. 2015, Akbar et al. 2014, Ghodake et al. 2016). More the dopant atoms diffuse in the host lattice it reduces the dislocations. However, probability that dopant atoms occupy interstitial positions and/or sit on grain boundaries increases at high dopant concentration of 8%. These atoms lead to destruction of crystalline order as was observed in Fig. 1.

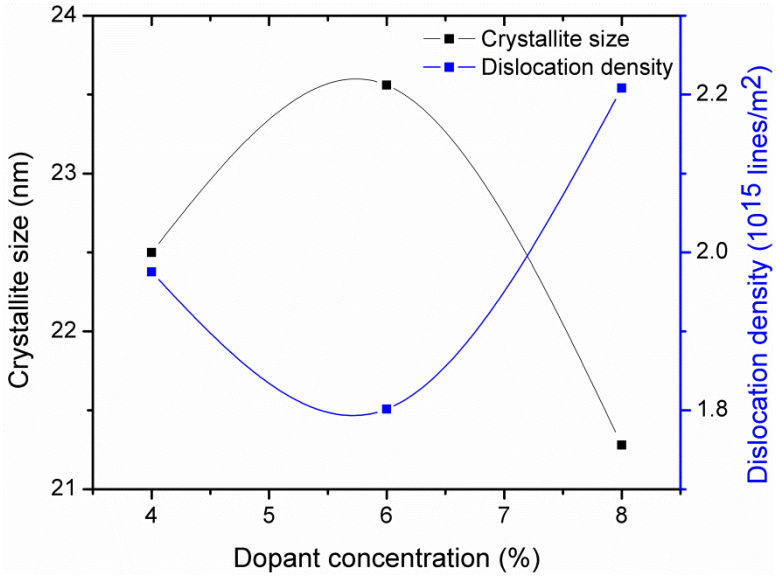

Fig. 2 Crystallite size and dislocation density plotted as a function of dopant concentration

Lattice parameters and unit cell volume are listed in table 1 for these aluminum doped hematite nanoparticles. Al^{3+} has six-coordinate ionic radius of 67.5pm that smaller than Fe^{3+} ions (74pm). So, decrease in lattice spacing and unit cell volume is observed with increase in dopant concentration. This consequently leads to increase in x-ray density.

Table 1 Structural parameters for aluminum doped iron oxide nanoparticles

Dopant concentration (%)	Lattice parameters (Å)		Unit cell volume ($Å^3$)	X-ray density ($g.cm^{-3}$)
	a	C		
4	5.015	13.620	296.6449	5.431539
6	5.010	13.615	295.945	5.444385
8	5.00	13.60	294.44	5.472213

Dielectric constant (ε) and tangent loss ($tan\ \delta$) were determined using Eqs. 4 and 5 (Barsoukov and Macdonald 2005).

$$\varepsilon = \frac{Cd}{\varepsilon_o A} \tag{4}$$

$$\tan\delta = \frac{1}{2\pi f \varepsilon_o \varepsilon \rho} \tag{5}$$

Where, *C* is the capacitance of films, d is the film thickness, ε_o is the permittivity of free space, A is the area, *f* is the frequency and *ρ* is the resistivity. Dielectric constant slightly decreases as frequency of applied field increases (log *f* < 6.5) as can be seen in Fig. 3(a). This decrease in dielectric constant is attributed to space charge polarization. Sources of space charges in polycrystalline specimen include lattice distortions and defects at grain boundaries. These space charge carriers make contribution to dielectric constant at high frequencies. But it can be seen that dielectric constant increases in the high frequency region (log f > 6.5). This increase in dielectric constant is associated with the resonance effect. This effect arises when mobility of space charge carriers matches with the frequency of externally applied field (Ghodake et al. 2016). On the other hand, tangent loss decreases as frequency of applied field increases and becomes constant at high frequencies. This behavior is in accordance with Maxwell Wagner two layered model. According to this model, dielectric specimen is composed of grain and grain boundaries where grains are more conducting as compared to grain boundaries. Role of grains dominate at high frequencies and grain boundaries are active at low frequencies (Riaz et al. 2015). This results in high tangent loss at low frequencies as can be seen in Fig. 3(b). High dielectric constant and low tangent loss at high frequencies makes these nanoparticles a potential candidate for high frequency applications.

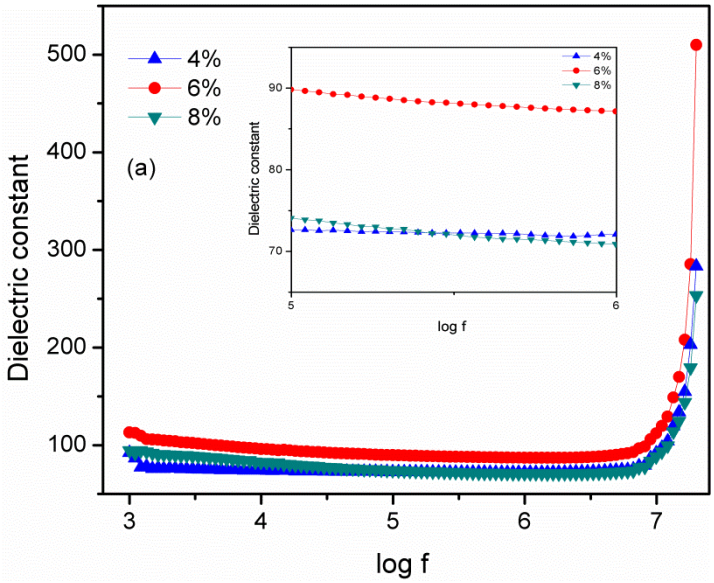

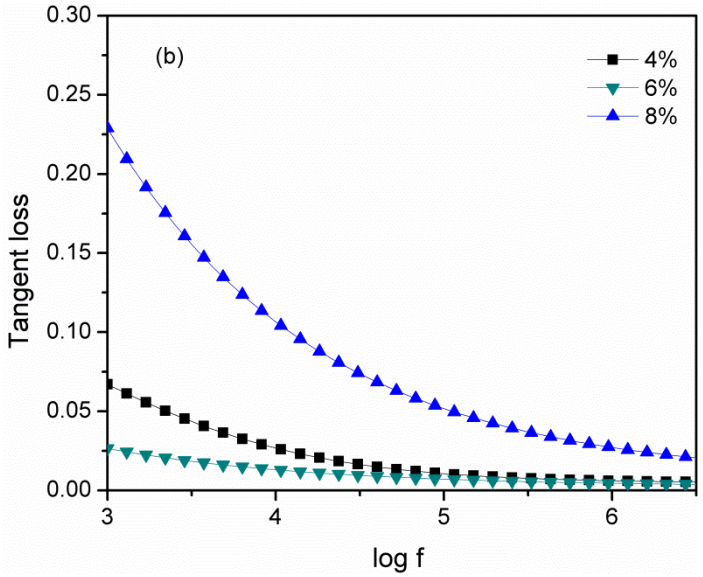

Fig. 3 (a) Dielectric constant (b) Tangent loss for aluminum doped iron oxide nanoparticles

Dielectric constant and tangent loss are plotted as a function of dopant concentration in Fig. 4. It can be seen that dielectric constant increases from 72 to 89.7 as dopant concentration was increased from 4% to 6%. Further increase in dopant concentration resulted in decrease in dielectric constant to 74 (log f = 5.0). The increase in dielectric constant is associated with increase in crystallite size as was observed in Fig. 2. This favors the formation of 180˚ domains as a result of which dielectric constant increases. Whereas, at high dopant concentration, partial clamping of domain wall motion can play critical role due to increased dislocations. This results in decrease in dielectric constant at high dopant concentration (Riaz et al. 2015).

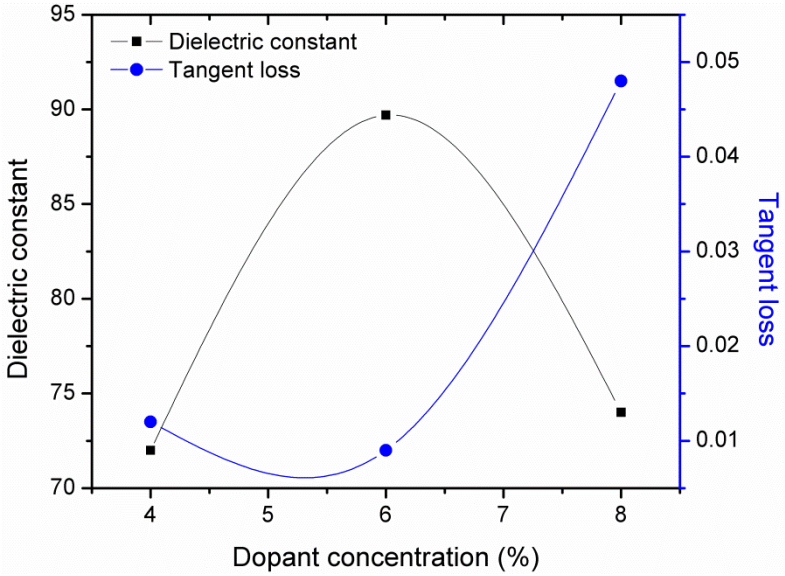

Fig. 4 Dielectric constant and tangent loss plotted as a function of dopant concentration

Conductivity (σ) of Al doped iron oxide nanoparticles was calculated using Eq. 6 (Barsoukov and Macdonald 2005).

$$\sigma = 2\pi f \varepsilon \varepsilon_o \tan\delta \quad (6)$$

Conductivity of Al doped iron oxide nanoparticles is plotted as a function of log f in Fig. 5. The conductivity remains constant in the low frequency region indicating contribution from d.c. conductivity. D.C. conductivity arises due to the presence of free pace charge carriers. At high frequencies, conductivity increases indicating the contribution from a.c. conductivity. A.C. conductivity is associated with bound charges that hop from one potential well to another (Jamal et al. 2011, Shinde et al. 2011).

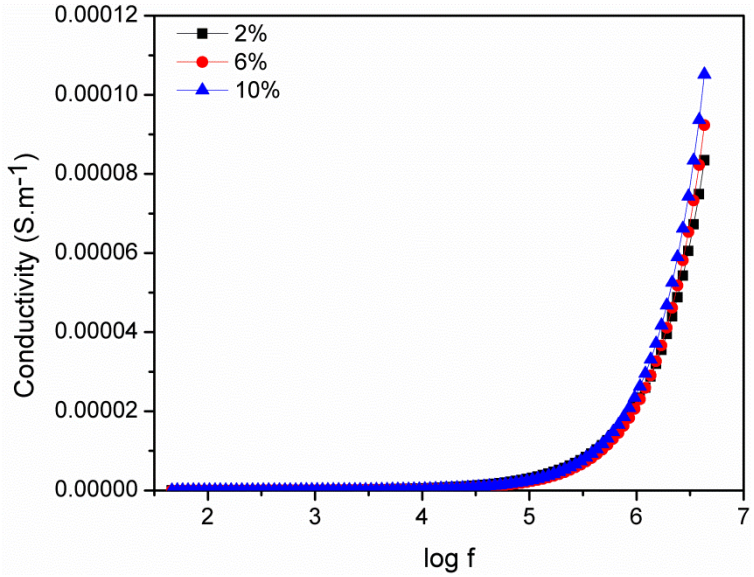

Fig. 5 Conductivity for Al doped hematite nanoparticles

Fig. 6 shows real and imaginary part of impedance for Al doped hematite nanoparticles plotted as a function of log *f*. It can be seen that real part of impedance (Z') decreases as frequency of applied field increases and becomes constant at high frequencies. Decrease in Z' at high frequencies is associated with increase in conductivity (Jamal et al. 2011) of Al doped hematite nanoparticles as was observed in Fig. 5. On the other hand, Z'' increases and attains a maximum value, known as relaxation peak, and then decreases at high frequencies. Relaxation process at low temperatures is attributed to the presence of immobile charge carriers (Jamal et al. 2011). Changes in width and position of relaxation peak indicate that dielectric relaxation phenomena are strongly affected by changes in dopant concentration.

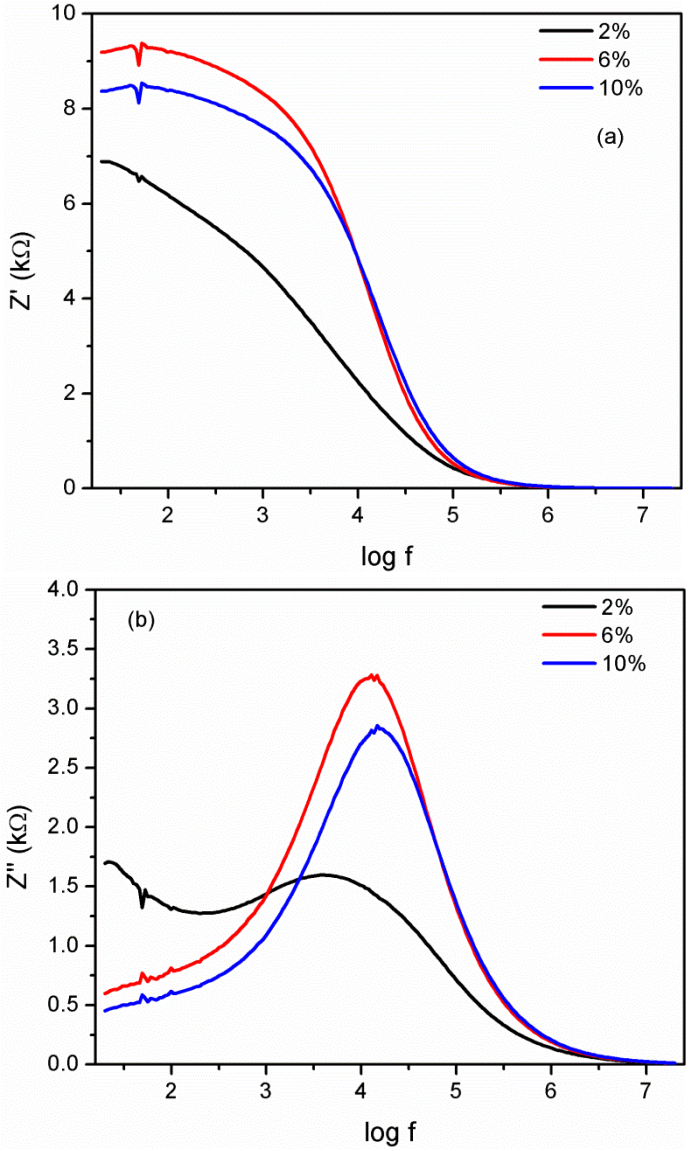

Fig. 6 (a) Real impedance (b) Imaginary impedance for Al doped hematite nanoparticles

4. CONCLUSIONS

Aluminum doped iron oxide nanoparticles were prepared using sol-gel method. Dopant concentration was varied as 4%, 6% and 8%. XRD results confirmed the formation of hematite phase of iron oxide. Crystallinity of nanoparticles decreased as dopant concentration was increased from 6% to 8% indicating that dopant atoms occupied sites at the grain boundaries. Dielectric constant increased from 72 to 89.7 (log f = 5.0) as dopant concentration was increased to 6%. Increase in dielectric constant and decrease in tangent loss at high frequencies indicate potential of these nanoparticles in high frequency applications. Real and imaginary part of impedance indicated that dielectric relaxation phenomena were strongly dependent on dopant concentration.

REFERENCES

Akbar, A. Riaz, S. Ashraf, R. and Naseem, S. (2014), “Magnetic and magnetization properties of Co-doped Fe_2O_3 thin films,” *IEEE Trans. Magn.*, **50**, 2201204

Aragon, F.F.H. Ardisson, J.D. Aquinoa, J.C.R. Gonzalez, I., Macedo, W.A.A., Coaquira, J.A.H., Mantilla, J., Silva, S.W. and Morais, P.C. (2016), “Effect of the thickness reduction on the structural, surface and magnetic properties of α-Fe_2O_3 thin films”, Thin Solid Films, **607,** 50–54.

Barsoukov, E. and Macdonald, J.R. (2005), “Impedance spectroscopy theory: Experiment and applications”, John Wiley & Sons, Inc., Publication, New Jersey, 2005.

Chakraborty, M. Ghosh, A. Thangavel, R. and Asokan, K. (2016), “Conduction mechanism in mesoporous hematite thin films using low temperature electrical measurements and theoretical electronic band structure calculations”, *J. Alloy Compd.*, **664**, 682-689

Cullity, B.D. (1956), “Elements of x-ray diffraction”, Addison Wesley Publishing Company, USA.

Ghodake, U.R. Chaudhari, N.D. Kambale, R.C. Patil, J.Y. and Suryavanshi, S.S. (2016), “Effect of Mn^{2+} substitution on structural, magnetic, electric and dielectric properties of Mg–Zn ferrites”, *J. Magn. Magn. Mater.*, **407**, 60–68

Glasscock, J.A. Barnes, P.R.F. Plumb, I.C. Bendavid, A. and Martin, P.J. (2008), “Structural, optical and electrical properties of undoped polycrystalline hematite thin films produced using filtered arc deposition”, *Thin Solid Films*, **516**, 1716–1724.

Jamal, E.M.A. Kumar, D.S. and Anantharaman, M.R. (2011), “On structural, optical and dielectric properties of zinc aluminate nanoparticles”, *Bull. Mater. Sci.*, **34**, 251–259.

Kumari, R. Sahai, A. and Goswami, N. (2015), “Effect of nitrogen doping on structural and optical properties of ZnO nanoparticles”, *Prog. Nat. Sci.: Mater. Int.*, **25**, 300–309.

Riaz, S. and Naseem, S. (2007), “Effect of reaction temperature and time on the structural properties of Cu(In,Ga)Se_2 thin films deposited by sequential elemental layer technique”, *J. Mater. Sci. Technol.*, **23**, 499-503.

Riaz, S. Akbar, A. and Naseem, S. (2014), “Ferromagnetic effects in Cr-Doped Fe_2O_3 thin films” *IEEE Trans. Magn.*, **50**, 2200704

Riaz, S. Shah, S.M.H. Akbar, A. Atiq, S. and Naseem, S. (2015), “Effect of Mn doping on structural, dielectric and magnetic properties of $BiFeO_3$ thin films”, *J. Sol-Gel Sci. Technol.*, **74**, 329-339.

Yang, T.I. Brown, R.N.C. Kempel, L.C. and Kofinas, P. (2010), “Surfactant-modified nickel zinc iron oxide/polymer nanocomposites for radio frequency applications”, *J. Nanopart. Res.*, **12**, 2967–2978.

Zhou, Z. Huo, P. Guo, L. and Prezhdo, O.V. (2015), “Understanding hematite doping with group IV elements: A DFT+U study”, *J. Phys. Chem. C*, **119**, 26303−26310.